First Principles Analysis of Ethylene Oligomerization on Single-site Ga^{3+} Catalysts Supported on Amorphous Silica

Yinan Xu[a], Nicole J. LiBretto[a], Guanghui Zhang[a, b], Jeffrey T. Miller[a], and Jeffrey Greeley[a]*

[a] Davidson School of Chemical Engineering, Purdue University, 480 Stadium Mall Drive, West Lafayette, Indiana 47907, United States

[b] State Key Laboratory of Fine Chemicals, PSU-DUT Joint Center for Energy Research, School of Chemical Engineering, Dalian University of Technology, Dalian, Liaoning Province 116024, P.R. China

Corresponding author: * jgreeley@purdue.edu (J. G.)

Abstract

Amorphous, single site, silica-supported main group metal catalysts have recently been found to promote olefin oligomerization with high activity at moderate temperatures and pressures (~250°C and 1 atm). Herein, we explore the molecular-level relationship between active site structures and the associated oligomerization mechanisms by developing amorphous, silica-supported Ga^{3+} models from periodic, first-principles calculations. Representative Ga^{3+} sites, including three- and four-coordinated geometries, are tested for multiple ethylene oligomerization pathways. We show that the three-coordinated Ga^{3+} site promotes oligomerization through a facile initiation process that generates a Ga-alkyl intermediate, followed by a Ga-alkyl-centered Cossee-Arlman mechanism. The strained geometry of a three-coordinated site enables a favorable free energy landscape with a kinetically accessible ethylene insertion transition state (1.7 eV) and a previously unreported β-hydride transfer step (1.0 eV) to terminate further C-C bond formation. This result, in turn, suggests that Ga^{3+} does not favor polymerization chemistry, while microkinetic modeling confirms that ethylene insertion is the rate-determining step. The study demonstrates a promising flexibility of main group ions for hydrocarbon transformations and, more generally, highlights the importance of the local geometry of metal ions on amorphous oxides in determining catalytic properties.

Introduction

Light olefins (ethylene and propylene) are the fundamental building blocks of the petrochemical industry. The molecules are readily available and can be converted to a wide range of useful intermediate and final products.[1–3] The production of short linear alpha olefins (LAOs), in particular, has been of significant interest in the olefin industry for the past few decades, as they form the key ingredients of various plastics, lubricants, fuels, and surfactants.[3–6] Production of LAOs, such as 1-butene, 1-hexene, and 1-octene, through selective catalytic olefin oligomerization has, in turn, become a core research topic in the olefin community due to the existence of many emerging alternative sources of light olefins and the increasing demand for polyethylene.[7–9] Presently, homogeneous catalysts, using ligand-modified transition metals, are among the most active and selective catalysts for olefin oligomerization.[10,11] Among the transition metals, nickel complexes are commonly used, where the Ni^{2+} compounds modified with alkyl or hydride moieties are the catalytic centers responsible for olefin oligomerization.[10–13] Many efforts have also been devoted to developing heterogeneous catalysts for olefin oligomerization, given their greater facility for catalyst regeneration and product separation. As an example, reactive transition metal species, inspired by analogous structures on homogeneous catalysts, can be supported on porous structures, such as zeolites and amorphous silica, but these catalysts suffer from poor oligomerization activity or low selectivity to LAOs.[14–19]

Density functional theory (DFT)-based studies are becoming increasingly important in elucidating the structures and properties of active sites, as well as the reaction mechanisms, of heterogeneously catalyzed olefin oligomerization processes.[20–22] For instance, a recent first-principles study by Brogaard *et al.* investigated Ni(0), Ni^{+}, and Ni^{2+} supported on an SSZ-24 framework in the context of ethylene oligomerization. The work revealed that the most plausible pathway starts from a [Ni(II)-ethylene-H]$^+$ complex, analogous to a Ni-alkyl ligand in the homogeneous context, and the oligomerization chemistry follows the classic Cossee-Arlman (C-A) mechanism, where ethylene coordinates and inserts between the species and the Ni ion, resulting in chain growth.[22] The process is terminated via an ethylene-assisted β-hydride elimination step that restores the [Ni(II)-ethylene-H]$^+$ moiety. In another mechanistic study by Metzger *et al.*, investigating Ni-MFU-4*l* for ethylene dimerization, a combination of isotope tracing, molecular probes, and DFT calculations were used to demonstrate that the catalytic cycle also follows a C-A mechanism, where ethylene insertion and β-hydride elimination are the key elementary steps.[23]

To expand the space of possible heterogeneous catalysts for olefin oligomerization, single-site, silica-supported main-group Ga ions have recently been explored and found to selectively catalyze ethylene and propylene oligomerization to higher molecular weight linear olefins, up to at least C_{18}, at 250 °C and an atmospheric pressure.[24] Through a combination of in-situ and ex-situ X-ray absorption spectroscopy (XAS), H/D exchange, IR techniques, and DFT calculations, it was determined that Ga^{3+} sites catalyze the oligomerization reaction. The mechanism starts from a site activation process, where a Ga^{3+}-O bond is activated, resulting in Ga-vinyl and Si-OH moieties (species 1 to 2, Fig. 1). After the activation step, ethylene insertion and β-hydride elimination occur, leading to butadiene and a Ga-hydride site (species 6_b, Fig. 1). The Ga-hydride was proposed to be responsible for the subsequent oligomerization cycle, following a C-A mechanism (cycle c, Fig. 1).[24]

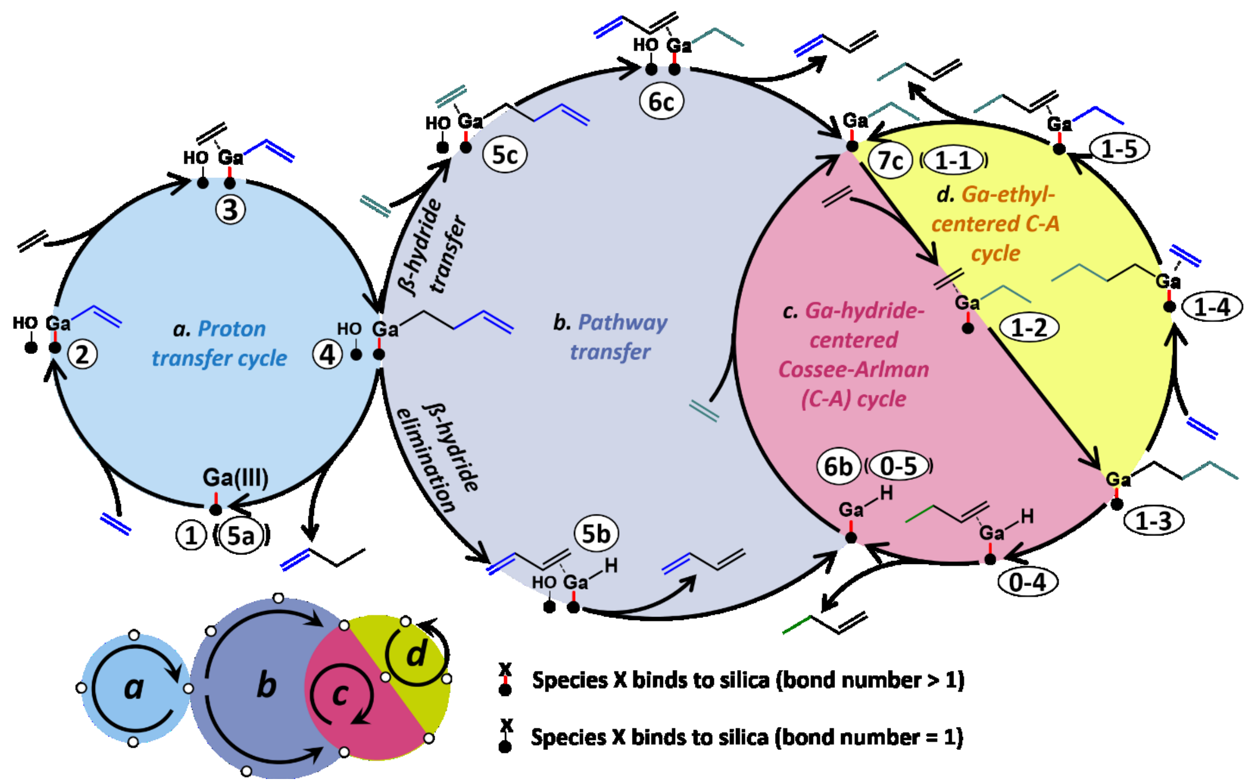

Figure 1. Possible ethylene oligomerization pathways on Ga^{3+}. Proton transfer cycle occurs on the empty Ga^{3+} site (region a); alternatively, formation of Ga-hydride or Ga-alkyl leads to pathway transfer (region b) to Cossee-Arlman mechanisms for ethylene oligomerization (either Ga-hydride-centered (region c) or Ga-alkyl-centered (region d)). The corresponding energies and geometries are shown in Figures 3-5.

To further elucidate the mechanistic and structural aspects of oligomerization on Ga-based silica catalysts, it is of interest to explore whether additional factors, such as the intrinsic heterogeneity of amorphous silica, can accommodate activation of other oligomerization pathways. It is well-known that many heterogeneous catalytic reactions are highly sensitive to the structure of active sites.[25–27] The Cr^{3+}-silica geometry in the Philips catalyst for ethylene polymerization is a useful example, wherein the reactivity of different Cr sites in terms of initiation, propagation, and termination energetics vary significantly with the local strain condition, causing a small percentage of the Cr sites to dominate the polymerization chemistry, [27–29] Further, in recent works, an alternate C-A cycle with alkene-assisted β-hydride transfer has been explored on both Ni, for oligomerization[22], and Cr, for polymerization,[30] and favorable energy landscapes are observed. Similar considerations may apply to the Ga^{3+}-silica system, underlining the need to further explore the link between oligomerization pathway selectivity and the structural diversity of the Ga^{3+} single-sites.

Herein, we develop amorphous silica-supported Ga^{3+} models based on periodic DFT calculations to study ethylene oligomerization mechanisms of the previously synthesized Ga/SiO_2 catalysts. The energetics of three primary cycles are compared, as shown in Figure 1. A proton transfer cycle can occur on the empty Ga^{3+} site starting from ethylene activation by Ga^{3+}, followed by insertion of another ethylene unit (species 1 to 4, Fig. 1). The Ga-butenyl species can then desorb via a proton transfer step, forming n-butene, completing the oligomerization cycle via proton transfer and reforming of the empty Ga^{3+} site (region a, Fig. 1).[30,31] Alternatively, the Ga-butenyl species may activate pathway transfer processes (region b, Fig. 1). β-hydride elimination can activate another oligomerization cycle, where butadiene and Ga-hydride are formed, proceeding to a C-A mechanism (species 4-6_b, Fig. 1). Further, as mentioned above, β-hydride elimination can be assisted by an incoming alkene molecule, which accepts a hydrogen atom and becomes an alkyl intermediate, which may be another key intermediate in the C-A cycle (species 4-7_c, Fig. 1). Following the pathway transfer process, the C-A cycle can be either Ga-hydride-centered (region c, Fig. 1) or Ga-alkyl-centered (region d, Fig. 1), and the two cycles differ by terminating the oligomer chain growth through β-hydride elimination or by directly transferring hydrogen to an ethylene molecule. In our Ga/SiO_2 system, we report that only the less-constrained, three-coordinated Ga^{3+} site is responsible for the oligomerization reactivity through the Ga-alkyl centered C-A cycle, of which the free energy landscape is significantly more favorable than the competing proton transfer and the hydride-centered C-A mechanisms. The selective ethylene dimerization observed in experiments is enabled by an unreported transition state of the ethylene-assisted β-hydride transfer step to terminate lengthening of the carbon backbone, and the activation energy is much lower than that of the ethylene insertion step. Finally, a detailed microkinetic analysis is carried out, based on the DFT results, which establishes that the ethylene insertion step is rate-limiting. In aggregate, these insights establish a comprehensive mechanistic understanding of how amorphous silica-supported main group single sites catalyze olefin oligomerization.

Methods

Single-site Ga^{3+}-silica structures are developed starting from a recently reported amorphous silica slab model.[32] The amorphous structure originates from an annealing procedure using molecular dynamics and continuous dehydration processes.[32] The periodic model has a sufficiently large unit cell to incorporate the possibility of long-range reconstructions and interactions (Figure 2). To create each single-atom Ga^{3+} site, a Si atom in the amorphous model is replaced with Ga, and a proton is added to an adjacent oxygen atom to maintain a charge balance.

The DFT calculations are based on self-consistent, periodic density functional theory using the Vienna Ab-initio Simulation Package (VASP).[33–36] The BEEF-VdW exchange-correlation functional[37] with projector augmented wave (PAW) pseudopotentials is employed.[38] A dipole layer is applied in the vacuum to eliminate the electrostatic interaction errors between mirror image slabs. A **k**-point grid of 2×2×1 is used based on Monkhorst-Pack **k**-sampling, and the convergence of the binding energy with respect to the **k**-point set is confirmed. A cutoff energy of 400 eV and a force-convergence criterion of 20 meV $Å^{-1}$ for local energy minimization are used. The climbing-image nudged-elastic-band (CINEB) method with seven intermediate images is used to locate the geometry of transition states[39,40], with initial guesses generated using the Image Dependent Pair Potential tool.[41] After the CINEB calculations converge to a force below 80 meV Å^{-1} for each image, the Lanczos diagonalization approach is employed to refine the transition state.[42] The force-convergence criterion of the Lanczos optimizations is 40 meV Å^{-1}.

Free energies are evaluated at 523 K and are calculated using the equation $G = E_{\mathrm{DFT}} + E_{\mathrm{ZPE}} - TS$, where E_{DFT} is the ground-state potential energy from DFT. The zero-point energy corrections (E_{ZPE}) are calculated from the harmonic vibrational states. For vibrational modes with wave numbers above 150 cm^{-1}, harmonic partition functions are employed to estimate entropies, while for modes with lower frequencies, particle-in-a-box (PIB) and free rotor schemes, depending on the geometric characteristics of the vibrations, are used (see Supporting Information for an example). The adsorption energies (G_{ads}) are referenced to empty sites (G_{Ga}) and appropriate amounts of gaseous ethylene molecules at 1 atm (G_{ethylene}). However, the free energy of Ga-hydride or Ga-alkyl moieties is used for the G_{Ga} term in the C-A cycles.

The microkinetic model simulates a continuous stirred-tank reactor (CSTR) with no concentration or temperature gradients. The reaction conditions used in the model are configured to be close to the experimental setup. Ethylene oligomerization is modeled at a temperature of 523 K and a total pressure of 1 atm. The reactor has a dimension of 1 cm × 1cm × 1 cm. The feed stream contains 20% of ethylene and 80% inert gas, and the feed volumetric flow rate is 1 cm^3 s^{-1}. The total number of available Ga sites is used to adjust the conversion of ethylene. Here, a total number of 0.85×10^{-4} mol of Ga sites per 1 g of catalyst is used, corresponding to a catalyst loading of 0.3%. We use this value because a Ga loading of 3 wt% was used in the experiments in the previous work, and we assume that approximately 10% of the total Ga sites are reactive.

Results and Discussion

Ga site creation

As mentioned in the Methods section, each single site Ga^{3+} ion in an amorphous silica model is introduced by a substitution technique, resulting in a Si-OH moiety. In total, five Si atoms, as shown in Figure S(1), are considered and substituted individually. Since a Si atom binds to four O atoms, there are four possible locations where a proton can be added. Therefore, a total of 20 DFT optimizations are performed to develop the Ga site structures for ethylene oligomerization on Ga/SiO_2.

As different Ga sites are created, the resulting oxygen atom of the Si-OH group can be either distant from, or close to, Ga. The possible extremes in active site structure are, in turn, represented by two Ga sites with substantially different Ga – Si-OH distances, and these are used as illustrative cases in the analysis that follows. In one case, the original Si-O bonds are elongated (Figure 2b: a=1.80 Å, b=1.66 Å, c=1.76 Å, and d=1.69 Å). As a result, the addition of hydrogen to the oxygen atom, leading to the cleavage of the bond (a), gives a final Ga-O distance of 4.57 Å after DFT optimization. In the second case, the Si atom used for creating the Ga site is located in a much more constrained framework, reflected by the shorter Si-O bonds (a=1.66 Å, b=1.62 Å, c=1.67 Å, and d=1.64 Å). As a result, the newly formed Si-OH group gives a Ga-O bond length of 2.02 Å. In the first of these cases, the Ga atom covalently binds to three oxygen atoms, which makes the Ga site three-coordinated. In the second case, the additional, short, Ga-Si-OH bond is considered as another coordination. Hence, the two extremes are defined as the three- and four-coordinated Ga sites (3CN and 4CN).

A complete list of Ga-hydroxyl distance of the 20 tested sites is included in the Supporting Information. We emphasize that the 3CN and 4CN sites, described above, bound the range of the calculated Ga-hydroxyl distances in all considered configurations. We also note that, in our experimental results, XAS on Ga/SiO_2 indicates that the majority of sites are Ga^{3+}, containing four Ga-O bonds, consistent with the 4CN site model. However, because XAS is a bulk technique, the possible formation of a small amount of 3CN Ga^{3+} sites (<10%) cannot be excluded,[24] and exploration of the catalytic relevance of these possible minority sites is a further motivation for the inclusion of the 3CN Ga sites in our analysis.

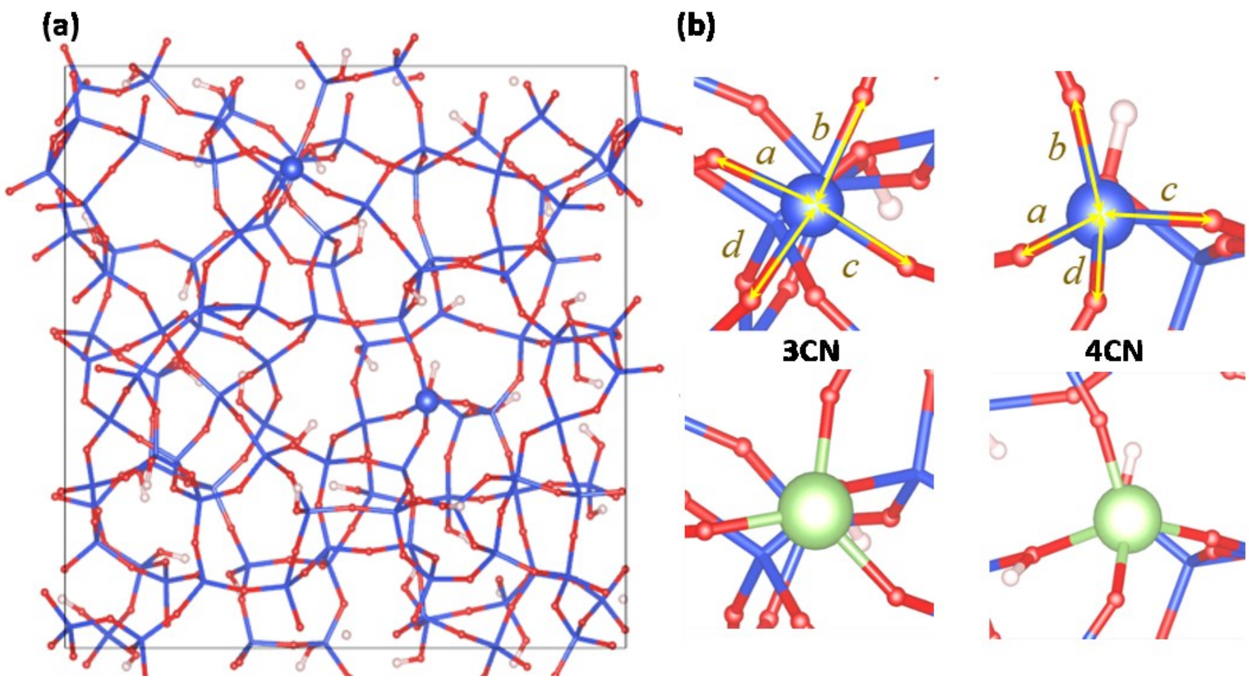

Figure 2. (a) Top view of unit cell of the amorphous silica model with locations of the Si atoms used for creating 3CN and 4CN sites, and (b) bonding conditions of the original Si atoms and corresponding Ga sites after DFT optimization (Ga=green, O=red, Si=blue, and H=white)

Ga^{3+} site activation process on 3CN site

Free energy diagrams of three pathways on the 3CN Ga site, evaluated at 523 K, are outlined in Figure 3a: the proton transfer mechanism (species 1 to 5_a in Fig. 1), and two pathway transfer processes forming either Ga-hydride (species 6_b) or Ga-alkyl (species 7_c) intermediates. The proton transfer step closes an oligomerization cycle and reforms the empty Ga site (region a, Fig. 1). The Ga-hydride and Ga-ethyl moieties are, in turn, key intermediates in the C-A oligomerization mechanism (regions c and d, Fig. 1).

Starting from the empty Ga site (species 1 in Fig. 4a), a C-H bond in ethylene is heterolytically cleaved, producing a vinyl group, and the resulting proton (H_a) from the cleavage goes to an oxygen (O_a) and breaks the Ga-O bond. The newly formed Si-OH group becomes distant from the Ga site, with a Ga-O distance of 4.2 Å. The heterolytic cleavage is exothermic, with a free energy change of -1.0 eV and an activation energy of 0.9 eV (step 1 to 2). Before the subsequent ethylene insertion occurs, a local energy minimum is found where ethylene is physisorbed on the Ga site (species 3). The C=C double bond coordinates to the planar, triangle geometry created by the Ga atom and two adjacent oxygen atoms (O_b and O_c). The physisorption is exothermic on the 3CN site (step 2 to 3, -0.2 eV), after which the migratory insertion of another ethylene molecule leads to a Ga-butenyl species with an activation barrier of 1.5 eV (step 3 to $‡^2$). In the transition state (species $‡^2$), the vinyl group rotates slightly towards the ethylene molecule and interacts with both Ga and a carbon atom (C_a), which eventually becomes the β-carbon of the Ga-butenyl species.

Pathway transfer on the 3CN site

As the C_4 intermediate forms, the ethylene-assisted β-hydride transfer is the most favorable pathway due to a generally lower free energy landscape (species 4 to 7_c, Fig. 3a). In this pathway, the physisorption of a third ethylene moiety is exothermic (step 4 to 5_c, -0.3 eV), and the activation barrier of β-hydride transfer is 0.8 eV (step 5_c to $‡^c$). Overall, the free energy of forming a Ga-ethyl intermediate from a clean 3CN Ga (species 1 in Fig. 4a) site is -1.7 eV, which is an exothermic process, and the Ga-ethyl species is thus quite likely to form. In contrast to this β-hydride transfer, high barriers are observed for both the proton transfer and the β-hydride elimination steps. Indeed, the proton transfer step entails recovery of the cleaved Ga-O bond, which is quite high in energy due to the strained nature of the 3CN site. We note, in passing, that similarly high activation barriers for β-hydride elimination have also been observed for Zn-propyl species during propane dehydrogenation.[43]

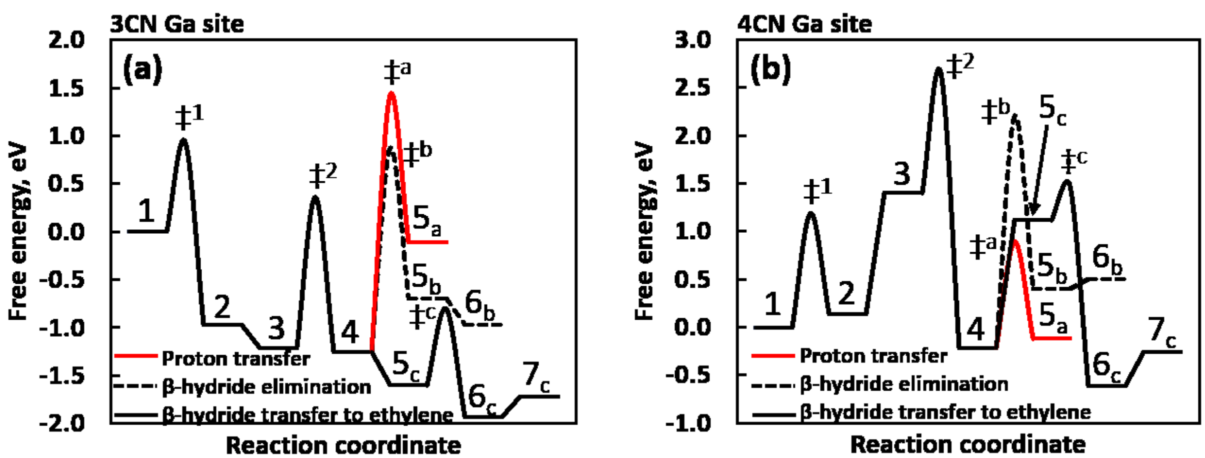

Figure 3. Free energy diagrams of proton transfer and pathway transfer (through β-hydride elimination and ethylene-assisted β-hydride transfer) processes on (a) 3CN and (b) 4CN Ga sites (T = 523 K). The adsorption energies are referenced to empty sites and appropriate amounts of gaseous ethylene molecules at 1 atm. The same species numbers are used in Figure 1.

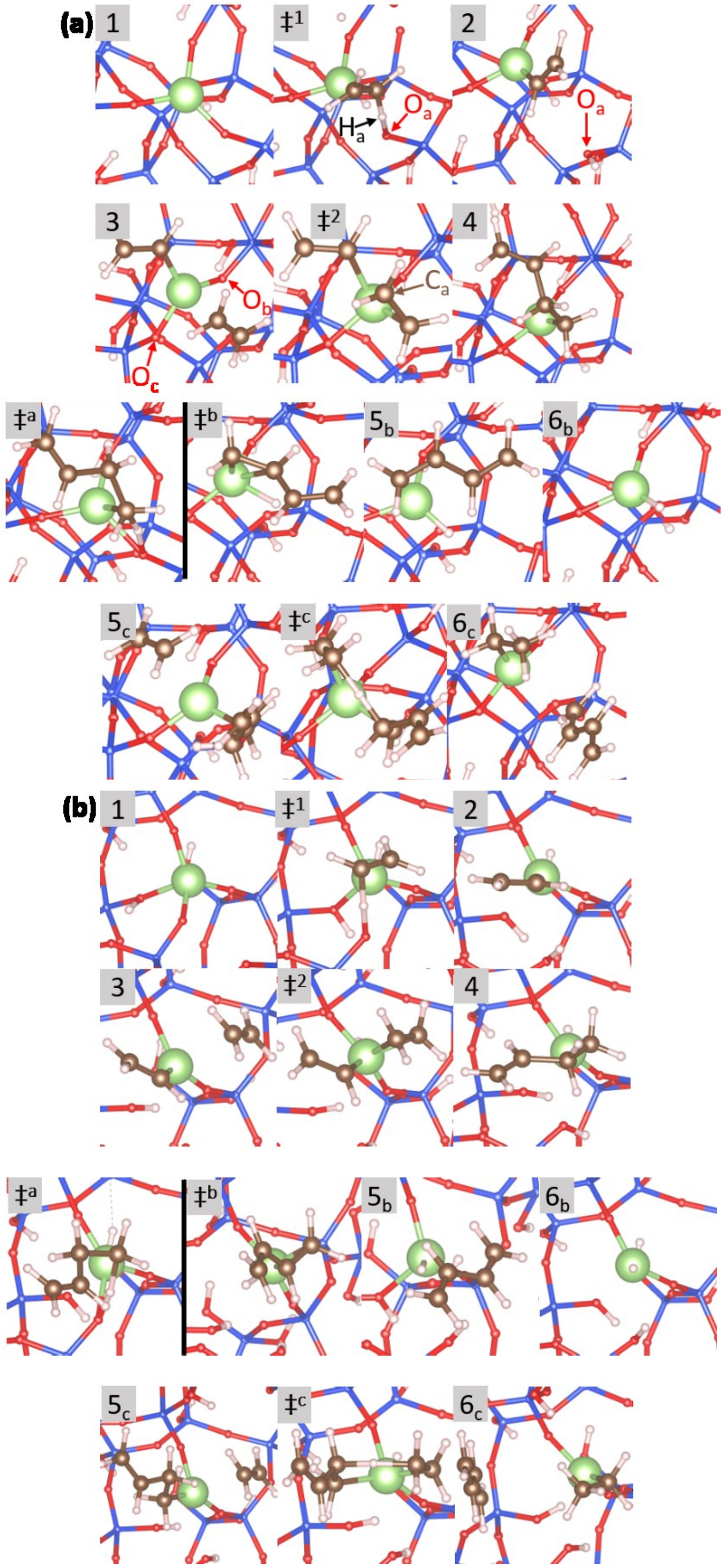

Figure 4. Schematics of proton transfer and pathway transfer on the (a) 3CN site and (b) 4CN Ga site (Ga=green, O=red, Si=blue C=black, and H=white, and the same species numbers are used in Figure 1.)

222

Proton transfer cycle vs. pathway transfer processes on the 4CN site

Free energy diagrams (523 K) of proton transfer (species 1 to 5_a, Fig. 1), β-hydride elimination (species 4 to 6_b), and ethylene-assisted β-hydride transfer (species 4 to 7_c) pathways on the 4CN Ga site are shown in Figure 3b. The 4CN Ga site has a different free energy landscape for site activation than does the 3CN site. Before the migratory insertion of ethylene, the physisorption step is greatly endothermic (step 2 to 3, +1.2 eV), which can be explained by a strong steric hindrance due to the nearby siloxane framework. Although a lower intrinsic activation barrier of ethylene insertion is found (step 3 to $‡^2$, +1.2 eV), the transition state is high in free energy if Ga-vinyl is used as a reference (3CN: 1.2 eV, 4CN: 2.5 eV). Similarly, the positive free energy change of ethylene physisorption leads to a significant unfavourability of ethylene-assisted β-hydride transfer (step 4 to 5_c, +1.3 eV), which is, in contrast, a viable pathway on 3CN Ga site. Since the 4CN Ga is in a more constrained environment, the Si-OH group formed due to ethylene activation is not far from the Ga site (2.7 Å, species 4), allowing for a relatively facile proton-transfer step to recover the original 4CN Ga site with an accessible activation barrier (step 4 to $‡^a$, 1.1 eV). Therefore, the 4CN site is more likely to catalyze olefin oligomerization through the proton transfer cycle, though a fairly low turnover frequency is expected due to the high barrier of olefin insertion. On the other hand, a pathway transfer to C-A mechanism is very likely to occur on the 3CN Ga site, forming a Ga-alkyl intermediate.

Olefin Oligomerization following a Cossee-Arlman mechanism on 3CN site

In the Ga site activation analysis on 3CN sites, the formation of a Ga-alkyl moiety through β-hydride transfer is the most energetically favorable pathway. Following the site activation, the coordination of an ethylene molecule to the alkyl group occurs, which initiates the C-A oligomerization cycle. Our analysis starts from the Ga-alkyl species, and Figure 5a shows the free energy diagram of C-A mechanism on a 3CN site. However, we analyze two types of C-A mechanisms (Figure 1) starting from either Ga-hydride or Ga-alkyl These configurations may, in principle, interconvert. We further analyze the related possibility that 3CN and 4CN sites may catalyze the C-A mechanism beginning with the Ga-hydride species, which can be produced with a hydrogen gas treatment.[24]

The ethylene physisorption on Ga-ethyl species is exothermic, with a free energy change of -0.3 eV (species 1-1 to 1-2). The migratory insertion of the second ethylene molecule, which approaches Ga and binds to the ethyl group, has an activation barrier of 1.7 eV (species 1-2 to 1-3). Following the physisorption of an additional ethylene molecule, the activation barrier of the β-hydride transfer (species 1-4 to 1-5, 1.0 eV) is much lower than that of the ethylene insertion step. The β-hydride transfer step finishes one catalytic cycle and reforms the Ga-alkyl species. We have also calculated the barrier of β-hydride elimination leading to the Ga-hydride moiety, for which the barrier is significantly higher than the ethylene-assisted barrier (species 1-3 to $\ddagger^b$, 2.4 eV), suggesting that the Ga-hydride is unlikely to form. Overall, based on the free energy analysis, we predict that Ga-alkyl favors the formation of short oligomers, since the termination step (β-hydride transfer) will be faster than the propagation step (migratory insertion) due to a much lower activation barrier. This behavior has been observed in the experiments, where butenes are the primary products detected. On the other hand, the C-A mechanism will not be dominated by the Ga-hydride spices, given a high barrier of β-hydride elimination step.

We highlight that the transition state geometry of β-hydride transfer on the 3CN Ga site is fundamentally different from the step occurring on a transition metal single site. In the transition states on Ni^{2+} or Cr^{3+} single sites, the hydrogen atom being transferred is close to the metal center, and this interaction contributes to the stabilization of transition state.[23,30] In the transition state on a 3CN Ga site ($\ddagger^{a}$), however, the hydrogen atom being transferred does not interact closely with the Ga atom, suggesting that Ga does not directly activate the C-H bond. Nevertheless, a low barrier is observed. This geometry was reported for early transition metal-based Ziegler-Natta catalysts, with an associated low barrier being attributed to a pseudo-hydrogen bond effect.[44,45] Our results suggest that a similar effect may extend to main group single sites, such as Ga.

Olefin oligomerization following the Cossee-Arlman mechanism on a 4CN site

The activation of ethylene on a 4CN Ga site generates a Si-OH group close to Ga. However, second Si-OH group is also present due to the original Ga site creation process (species 2 in Figure 4b). The close proximity of the two Si-OH groups leads to the possibility of a dehydration step, which gives an oxygen bridged Si pair and a water molecule. The free energy of dehydration is reasonably negative when water is present at low pressures ($P_{\mathrm{water}} = 10^{-9}$ atm, calculations included in Supporting Information). The dehydration step can occur as soon as ethylene is activated, and since the two Si-OH groups are removed, the proton transfer pathway, reforming the original 4CN Ga site, would no longer be viable. As with the 3CN site, β-hydride transfer to ethylene would then lead to C-A mechanism dominated by a Ga-ethyl species (see free energy diagram in Supporting Information).

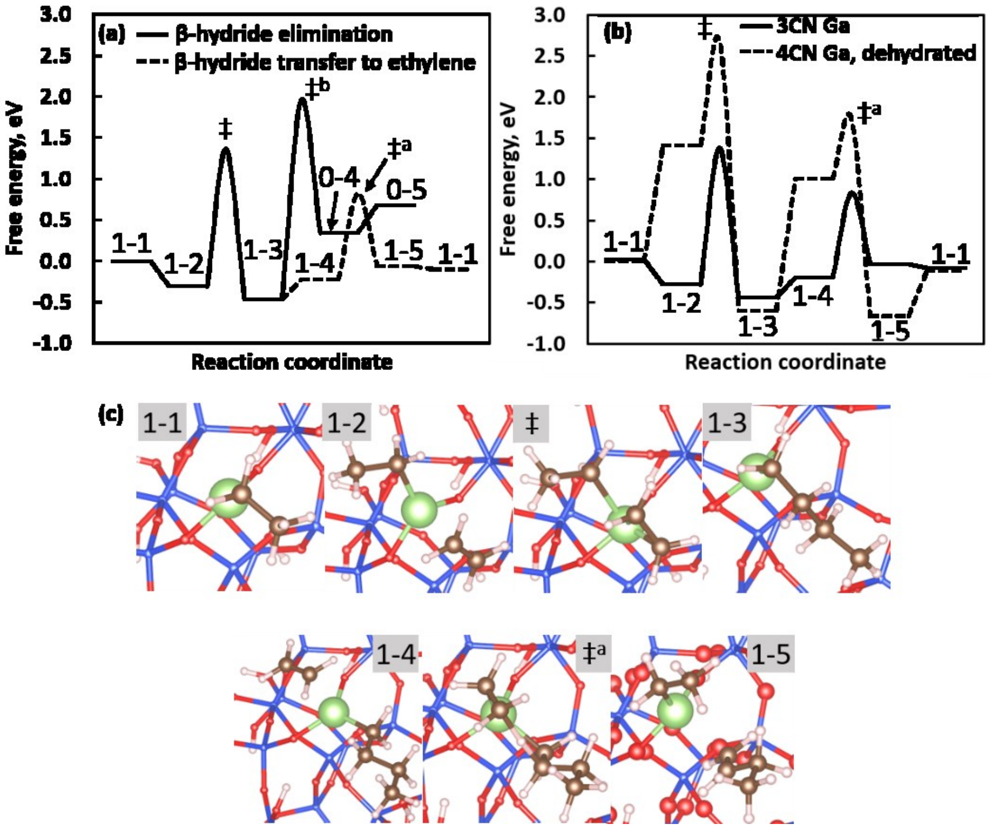

Figure 5. (a) Free energy diagrams of ethylene oligomerization with β-hydride elimination compared to β-hydride transfer pathways on 3CN Ga sites (T = 523 K), (b) Free energy diagrams of ethylene oligomerization on 3CN and 4CN sites with dehydration, and (c) Schematics of ethylene oligomerization intermediates on a 3CN site (T = 523 K). The adsorption energies are referenced to Ga-ethyl species and appropriate amounts of gaseous ethylene molecules at 1 atm. The same species numbers are used in Figure 1.

Figure 5b shows the energetics of the C-A oligomerization cycle on the two sites: 3CN, and the 4CN Ga with a dehydration step. Among them, the 3CN site generally exhibits a much more favorable energy landscape. Specifically, low activation barriers of both ethylene migratory insertion (3CN: 1.7 eV) and β-hydride transfer (3CN: 1.0 eV) are observed. On the 4CN dehydrated site, the ethylene physisorption steps before insertion and β-hydride transfer have positive changes in free energies (1.4 and 1.6 eV, respectively), leading to significantly higher overall barriers of ethylene insertion.

Olefin oligomerization following Ga-hydride-centered Cossee-Arlman mechanism

As discussed above, a C-A mechanism can possibly be Ga-hydride-centered (region c, Fig. 1), and these sites could be produced through a hydrogen gas treatment.[24] To explore this possibility, we have analyzed the free energy landscapes of the Ga-hydride-centered C-A mechanism on both 3CN and 4CN sites (Figs. S5-7). High activation barriers are involved in the β-hydride elimination steps (4CN: 2.5 eV, 3CN: 2.3 eV), and the alternative β-hydride transfer, producing Ga-ethyl, exhibits much lower activation barriers. Further, high activation barriers of ethylene insertion are consistently observed for the 4CN sites (2.9 eV). Therefore, we predict that the Ga-ethyl-centered C-A mechanism is the most favorable pathway on the Ga/SiO_2 system, and the 3CN Ga sites exhibit a much higher turnover frequency than the 4CN ones. Hence, the 3CN sites likely have a major effect on the overall reactivity of the catalyst.

Microkinetic modeling

Microkinetic modeling enables a direct comparison of the predicted rates and coverages of distinct surface sites. We note that this information is not easily obtained through experiments, given the site diversity in amorphous silica. Kinetic parameters are predicted from the free energy diagram of the 3CN site, and 10% of the Ga sites in the experimental loading are assumed to be active. We only include the Ga-alkyl-centered C-A cycle because the DFT results have indicated that other cycles will not contribute to the rate or selectivity. With a pure ethylene feed, a conversion of 0.5% is predicted at 523 K and a total pressure of 1 atm, and the turnover frequency (TOF) is 5.7×10^{-3} s^{-1} (with a dilute feed - 20% ethylene - an ethylene conversion of 1.4% is obtained at 523 K and a total pressure of 1 atm, and a similar TOF, 3.2×10^{-3} s^{-1}, is observed). The computational values are higher than the experimental value (0.9×10^{-3} s^{-1}). However, we highlight that the experimental values assume that all Ga sites are active, and hence this value is likely a lower limit on the true turnover frequency. Considering that Ga sites in the synthesized sample are, on average, four-coordinated, a relatively small percentage of 3CN sites are likely to be present in the sample and are responsible for the oligomerization chemistry. Indeed, we predict that the 4CN sites exhibit extremely low turnover frequencies due to the endothermic nature of ethylene physisorption steps, as well as a high barrier of ethylene insertion.

We also performed a degree of rate control (DRC) analysis to confirm our prediction of rate-limiting step by evaluating the sensitivity of each elementary step to the overall turnover frequency. The DRC analysis has been performed on all steps in an ethylene oligomerization cycle, leading to the conclusion that the ethylene migratory insertion step, having a DRC for 1-butene formation of 0.95, is the rate-determining step. The turnover frequency is much less sensitive to the β-hydride transfer step, whose DRC values are in the order of 10^{-2}. In the results of the dilute feed, the most abundant surface intermediates (MASI) are physisorbed ethylene and Ga-n-butyl species (coverages: 0.54 and 0.46, respectively). The results are consistent with the free energy analysis, where the two species represent reasonable free energy wells. The physisorption step has a negative free energy, and given a relatively high barrier of ethylene insertion, ethylene would accumulate before the elementary step occurs, leading to its higher coverage. Consistent results are obtained using the pure feed, where the physisorbed ethylene on the Ga-ethyl species has an even higher coverage (coverage: 0.99), and the ethylene insertion step remains the rate determining step (DRC: 0.94). Using a simplified rate expression by assuming ethylene insertion being rate-determining, an Arrhenius plot from microkinetic modeling is included in the Supporting Information (Fig. S10), where the apparent activation energy from the free energy analysis is reproduced. This further confirms that the other elementary steps can be treated as quasi-equilibration.

Conclusions

We present a first-principles study of ethylene oligomerization on single-site Ga^{3+} catalysts supported on amorphous silica. Energetics of multiple oligomerization pathways are compared on two representative sites: 3CN and 4CN Ga. Although the 4CN sites may in principle promote the ethylene oligomerization cycle through a proton transfer cycle, they are not likely to be responsible for experimentally observed reactivity due to a high ethylene insertion barrier. The 3CN Ga site, however, yields a much more favorable energy landscape, which starts from a site activation process to form a Ga-alkyl species, followed by a Ga-alkyl-centered Cossee-Arlman mechanism. With a lower termination barrier than the ethylene insertion step, the 3CN Ga sites favor selective ethylene oligomerization to short oligomers, consistent with the experimental results at 250 °C and 1 atm. Microkinetic modeling results confirm that the ethylene insertion step is rate-limiting. Further, we note that the in the transition state of the facile β-hydride transfer step, an unusual geometry is found for the main group Ga catalyst, where the hydrogen being transferred does not interact with Ga center. This study highlights the capability of a oxide-supported main group metals to perform olefin oligomerization and also provides suggestions to design such catalysts, where the local coordination environment of Ga sites may be tuned to improve the catalyst activity.

Supporting Information

This material contains detailed free energy information of the analyzed reaction mechanisms, kinetic calculation details, entropy calculations, Ga site schematics, and Arrhenius plots.

Author Information

Corresponding Author

Jeffrey Greeley – *Davidson School of Chemical Engineering, Purdue University, West Lafayette, Indiana, 47907*

*Email: jgreeley@purdue.edu

Author Contributions

The manuscript was written through contributions of all authors. All authors have given approval to the final version of the manuscript.

ORCID

Yinan Xu: 0000-0002-5824-3502

Jeffrey Greeley: 0000-0001-8469-1715

Notes

The authors declare no competing financial interest.

Acknowledgments

This paper is based upon work supported in part by the National Science Foundation through the Center for Innovative and Sustained Transformation of Alkane Resources (CISTAR) under Cooperative Agreement No. EEC-1647722. Use of the Center for Nanoscale Materials, an Office of Science user facility, was supported by the U.S. Department of Energy, Office of Science, Office of Basic Energy Sciences, under Contract No. DE-AC02- 06CH11357. Use of the National Energy Research Scientific Computing Center is also gratefully acknowledged. Y.X. and J.G. would like to thank Prof. Brandon C. Bukowski at Johns Hopkins University and Dr. Junnan Shangguan at UC Berkeley for insightful discussions.

References

1. Skupińska J. Oligomerization of α-Olefins to Higher Oligomers. *Chem Rev*. 1991;91(4):613-648. doi:10.1021/cr00004a007
2. Hulea V, Fajula F. Ni-exchanged AlMCM-41 - An efficient bifunctional catalyst for ethylene oligomerization. *J Catal*. 2004;225(1):213-222. doi:10.1016/j.jcat.2004.04.018
3. McGuinness DS. Olefin oligomerization via metallacycles: Dimerization, trimerization, tetramerization, and beyond. *Chem Rev*. 2011;111(3):2321-2341. doi:10.1021/cr100217q
4. Sydora OL. Selective Ethylene Oligomerization. *Organometallics*. 2019;38(5):997-1010. doi:10.1021/acs.organomet.8b00799
5. Leeuwen PWNM Van, Clément ND, Tschan MJ. New processes for the selective production of 1-octene. *Coord Chem Rev*. 2011;255(13-14):1499-1517. doi:10.1016/j.ccr.2010.10.009
6. Nicholas CP. Applications of light olefin oligomerization to the production of fuels and chemicals. *Appl Catal A Gen*. 2017;543(June):82-97. doi:10.1016/j.apcata.2017.06.011
7. Speiser F, Braunstein P, Saussine L. Catalytic ethylene dimerization and oligomerization: recent developments with nickel complexes containing P,N-chelating ligands. *Acc Chem Res*. 2005;38(10):784-793. doi:10.1021/ar050040d
8. Metzger ED, Brozek CK, Comito RJ, Dinca M. Selective dimerization of ethylene to 1-butene with a porous catalyst. *ACS Cent Sci*. 2016;2(3):148-153. doi:10.1021/acscentsci.6b00012
9. Finiels A, Fajula F, Hulea V. Nickel-based solid catalysts for ethylene oligomerization-a review. *Catal Sci Technol*. 2014;4(8):2412-2426. doi:10.1039/c4cy00305e
10. Keim W. Oligomerization of ethylene to α-olefins: Discovery and development of the shell higher olefin process (SHOP). *Angew Chemie - Int Ed*. 2013;52(48):12492-12496.

doi:10.1002/anie.201305308

11. Killian CM, Johnson LK, Brookhart M. Preparation of linear α-olefins using cationic nickel(II) α-diimine catalysts. *Organometallics*. 1997;16(10):2005-2007. doi:10.1021/om961057q

12. Speiser F, Braunstein P, Saussine L. Nickel complexes bearing new P,N-phosphinopyridine ligands for the catalytic oligomerization of ethylene. *Organometallics*. 2004;23(11):2633-2640. doi:10.1021/om034203i

13. Britovsek GJP, Malinowski R, McGuinness DS, et al. Ethylene Oligomerization beyond Schulz–Flory Distributions. *ACS Catal*. 2015;5(11):6922-6925. doi:10.1021/acscatal.5b02203

14. Martínez A, Arribas MA, Concepción P, Moussa S. New bifunctional Ni-H-Beta catalysts for the heterogeneous oligomerization of ethylene. *Appl Catal A Gen*. 2013;467:509-518. doi:10.1016/j.apcata.2013.08.021

15. Andrei RD, Popa MI, Fajula F, Hulea V. Heterogeneous oligomerization of ethylene over highly active and stable Ni-AlSBA-15 mesoporous catalysts. *J Catal*. 2015;323:76-84. doi:10.1016/j.jcat.2014.12.027

16. Lin S, Shi L, Zhang H, et al. Tuning the pore structure of plug-containing Al-SBA-15 by post-treatment and its selectivity for C16 olefin in ethylene oligomerization. *Microporous Mesoporous Mater*. 2014;184:151-161. doi:10.1016/j.micromeso.2013.10.016

17. Heveling J, Nicolaides CP, Scurrell MS. Catalysts and conditions for the highly efficient, selective and stable heterogeneous oligomerisation of ethylene. *Appl Catal A Gen*. 1998;173(1):1-9. doi:10.1016/S0926-860X(98)00147-1

18. Lallemand M, Finiels A, Fajula F, Hulea V. Continuous stirred tank reactor for ethylene

oligomerization catalyzed by NiMCM-41. *Chem Eng J*. 2011;172(2-3):1078-1082. doi:10.1016/j.cej.2011.06.064

19. Lallemand M, Rusu OA, Dumitriu E, Finiels A, Fajula F, Hulea V. NiMCM-36 and NiMCM-22 catalysts for the ethylene oligomerization: Effect of zeolite texture and nickel cations/acid sites ratio. *Appl Catal A Gen*. 2008;338(1-2):37-43. doi:10.1016/j.apcata.2007.12.024

20. Govindasamy A, Markova VK, Genest A, Rösch N. Ethene hydrogenation: Vs. dimerization over a faujasite-supported [Rh(C2H4)2] complex. A computational study of mechanism. *Catal Sci Technol*. 2017;7(1):102-113. doi:10.1039/c6cy02147f

21. Brogaard RY, Kømurcu M, Dyballa MM, et al. Ethene Dimerization on Zeolite-Hosted Ni Ions: Reversible Mobilization of the Active Site. *ACS Catal*. 2019;9(6):5645-5650. doi:10.1021/acscatal.9b00721

22. Brogaard RY, Olsbye U. Ethene Oligomerization in Ni-Containing Zeolites: Theoretical Discrimination of Reaction Mechanisms. *ACS Catal*. 2016;6(2):1205-1214. doi:10.1021/acscatal.5b01957

23. Metzger ED, Comito RJ, Hendon CH, Dincă M. Mechanism of single-site molecule-like catalytic ethylene dimerization in Ni-MFU-4l. *J Am Chem Soc*. 2017;139(2):757-762. doi:10.1021/jacs.6b10300

24. LiBretto NJ, Xu Y, Quigley A, et al. Olefin oligomerization by main group Ga3+ and Zn2+ single site catalysts on SiO2. *Nat Commun*. 2021;12(1):1-9. doi:10.1038/s41467-021-22512-6

25. Das U, Zhang G, Hu B, et al. Effect of Siloxane Ring Strain and Cation Charge Density on the Formation of Coordinately Unsaturated Metal Sites on Silica: Insights from Density

Functional Theory (DFT) Studies. *ACS Catal*. 2015;5(12):7177-7185. doi:10.1021/acscatal.5b01699

26. Praveen CS, Borosy AP, Copéret C, Comas-Vives A. Strain in Silica-Supported Ga(III) Sites: Neither Too Much nor Too Little for Propane Dehydrogenation Catalytic Activity. *Inorg Chem*. 2021;60(10):6865-6874. doi:10.1021/acs.inorgchem.0c03135

27. Goldsmith BR, Peters B, Johnson JK, Gates BC, Scott SL. Beyond Ordered Materials: Understanding Catalytic Sites on Amorphous Solids. *ACS Catal*. 2017;7(11):7543-7557. doi:10.1021/acscatal.7b01767

28. Floryan L, Borosy AP, Núñez-Zarur F, Comas-Vives A, Copéret C. Strain effect and dual initiation pathway in CrIII/SiO2polymerization catalysts from amorphous periodic models. *J Catal*. 2017;346:50-56. doi:10.1016/j.jcat.2016.11.037

29. Kaminsky W. *Polyolefins: 50 Years after Ziegler and Natta II*. Vol 258.; 2013. doi:10.1007/978-3-642-40805-2

30. Fong A, Yuan Y, Ivry SL, Scott SL, Peters B. Computational kinetic discrimination of ethylene polymerization mechanisms for the Phillips (Cr/SiO2) catalyst. *ACS Catal*. 2015;5(6):3360-3374. doi:10.1021/acscatal.5b00016

31. Delley MF, Núñez-Zarur F, Conley MP, et al. Erratum: Proton transfers are key elementary steps in ethylene polymerization on isolated chromium(III) silicates (Proceedings of the National Academy of Sciences of the United States of America (2015) 112:32 (E4505))). *Proc Natl Acad Sci U S A*. 2015;112(32):E4505. doi:10.1073/pnas.1512495112

32. Comas-Vives A. Amorphous SiO2 surface models: Energetics of the dehydroxylation process, strain, ab initio atomistic thermodynamics and IR spectroscopic signatures. *Phys*

Chem Chem Phys. 2016;18(10):7475-7482. doi:10.1039/c6cp00602g

33. Kresse G, Furthmüller J. Efficiency of ab-initio total energy calculations for metals and semiconductors using a plane-wave basis set. *Comput Mater Sci*. 1996;6(1):15-50. doi:10.1016/0927-0256(96)00008-0

34. Kresse G, Furthmüller J. Efficient iterative schemes for ab initio total-energy calculations using a plane-wave basis set. *Phys Rev B - Condens Matter Mater Phys*. 1996;54(16):11169-11186. doi:10.1103/PhysRevB.54.11169

35. Kresse G, Hafner J. Ab initio molecular dynamics for liquid metals. *Phys Rev B*. 1993;47(1):558-561. doi:10.1103/PhysRevB.47.558

36. Kresse G, Hafner J. Ab initio molecular-dynamics simulation of the liquid-metalamorphous- semiconductor transition in germanium. *Phys Rev B*. 1994;49(20):14251-14269. doi:10.1103/PhysRevB.49.14251

37. Wellendorff J, Lundgaard KT, Møgelhøj A, et al. Density functionals for surface science: Exchange-correlation model development with Bayesian error estimation. *Phys Rev B - Condens Matter Mater Phys*. 2012;85(23):32-34. doi:10.1103/PhysRevB.85.235149

38. Joubert D. From ultrasoft pseudopotentials to the projector augmented-wave method. *Phys Rev B - Condens Matter Mater Phys*. 1999;59(3):1758-1775. doi:10.1103/PhysRevB.59.1758

39. Henkelman G, Jónsson H. Improved tangent estimate in the nudged elastic band method for finding minimum energy paths and saddle points. *J Chem Phys*. 2000;113(22):9978-9985. doi:10.1063/1.1323224

40. Henkelman G, Uberuaga BP, Jónsson H. Climbing image nudged elastic band method for finding saddle points and minimum energy paths. *J Chem Phys*. 2000;113(22):9901-9904.

doi:10.1063/1.1329672

41. Smidstrup S, Pedersen A, Stokbro K, Jónsson H. Improved initial guess for minimum energy path calculations. *J Chem Phys*. 2014;140(21). doi:10.1063/1.4878664

42. Olsen RA, Kroes GJ, Henkelman G, Arnaldsson A, Jónsson H. Comparison of methods for finding saddle points without knowledge of the final states. *J Chem Phys*. 2004;121(20):9776-9792. doi:10.1063/1.1809574

43. Schweitzer NM, Hu B, Das U, et al. Propylene hydrogenation and propane dehydrogenation by a single-site Zn2+ on silica catalyst. *ACS Catal*. 2014;4(4):1091-1098. doi:10.1021/cs401116p

44. Novaro O, Chow S, Magnouat P. Mechanism of oligomerization of α-olefins with Ziegler-Natta catalysts. *J Catal*. 1976;41(1):91-100. doi:10.1016/0021-9517(76)90204-9

45. Cavallo L, Guerra G. A density functional and molecular mechanics study of β-hydrogen transfer in homogeneous Ziegler-Natta catalysis. *Macromolecules*. 1996;29(8):2729-2737. doi:10.1021/ma9511412